# Numerical analysis of a Kaplan turbine model during transient operation

IOP Conf. Series: Earth and Environmental Science **240** (2019) 022046 doi:10.1088/1755-1315/240/2/022046

# Numerical analysis of a Kaplan turbine model during transient operation

**R G Iovănel[1, 2], D M Bucur[1], G Dunca[1], M J Cervantes[2]**

[1] University Politehnica of Bucharest, Romania
[2] Luleå University of Technology, Luleå, Sweden

Raluca.iovanel@gmail.com

**Abstract**. Hydropower plants are currently being intensively employed for electrical grid regulation. As a consequence, the frequency of start/stops and load variations is considerably increasing, leading to the operation of hydraulic turbines under improper conditions. During the last years, studies have focused on Francis turbines. The present paper aims to investigate a Kaplan turbine model. The flow through the turbine is modelled during transient operation, from the best efficiency point to a part load operating point, using a moving mesh for the guide vane displacement. The simulations are validated against experimental velocity profiles. A time step sensitivity analysis is performed in order to determine the optimum discretization time. The possibility of using large time steps is explored. The numerically simulated unsteady pressure pulsations on the runner blades are analysed. The influence of the inlet boundary conditions on the accuracy of numerical simulations is studied. The results show that a linear flow rate variation defined during the guide vane closure leads to an overestimation of the turbine head compared to the experimental value due to an overestimation of losses. The second type of boundary conditions, a constant total pressure, results in an underestimation of the flow rate compared to the experimental value due again to an overestimation of the losses.

## 1. Introduction

The instability of the energy market is becoming a general concern due to the fluctuations introduced by the intermittent renewable energy sources. Hydropower plants represent the main solution to grid regulation therefore they are experiencing frequently changing operating conditions. Kaplan turbines are double-regulated turbines and can provide high efficiency over a wide range of flow rates and heads, a very important aspect regarding the grid regulation challenge. However, due to the fluctuating energy demand, the turbines are often operated under unfavorable conditions such as load variations, start/stops and away from the best efficiency point (BEP). Therefore, it is mandatory to consider the new operating conditions during the design stage or the refurbishment of hydraulic turbines.

Experimental campaigns such as the projects Francis-99 [1] and Bulb T [2] aimed for a better understanding of the flow structures developing inside hydraulic turbines during load variations [3, 4] or complete starts and stops of the machines [5, 6]. Concerning Kaplan turbines, there are several experimental studies available in the literature. The steady-state operation at BEP and off-cam operating points, i.e., a fixed runner blade angle, was investigated by Mulu et al. [7, 8] and Amiri et al. [9, 10]. An analysis of the load variation effects on a Kaplan turbine model was presented by Amiri et al. [11, 12]. Experimental studies are however limited due to large costs associated, problematic access to the geometry of the machines and restricted amount of information acquired. Computational Fluid Dynamics (CFD) is a reliable alternative or preferably, a complementary mean of research [13, 14].

Numerical studies, focusing predominantly on Francis type turbines, have been carried out in order to investigate both steady-state operations [15-16] and load variations [17] of hydraulic turbines. However, numerical simulations have disadvantages as well. A compromise must be achieved between the accuracy of the model and the mesh quality. The selection of the time step is also a sensitive decision. According to the Nyquist criteria, the maximum frequency of the phenomena captured by the numerical simulation represents half of the sampling frequency. Given the large Reynolds numbers that characterize the turbulent flow inside the turbines, the pressure and velocity fluctuations have high frequencies. Therefore, the numerical analysis requires a small time step, a long simulation time and a large amount of computational resources. According to Nicolle et al. [18] the computational domain may be reduced by using periodic interfaces and modelling only one blade passage (guide vane and/or runner blade) under the assumption that the flow is axisymmetric. The definition of the inlet boundary conditions is very important in order to correctly estimate the head losses inside the draft tube of an axial turbine [19]. The Reynolds Averaged Navier-Stokes turbulence models (RANS), which are the least computational expensive, are overpredicting the pressure losses, affecting the accuracy of numerical simulations [20].

In the present numerical analysis, two types of inlet boundary conditions are considered in order to evaluate the extent to which the definition of the boundary conditions influences the accuracy of numerical simulations. A time step sensitivity analysis is also performed.

## 2. Experimental and numerical test case – Porjus U9

### *2.1. General*

The test case employed in the present work is the Porjus U9 Kaplan turbine model, located in Älvkarleby, Sweden. The diameter of the runner is 0.5 m and the rotational speed is 696.3 rpm. The turbine model includes a spiral casing, a distributor composed of 18 stay vanes and 20 guide vanes, a runner with 6 blades, and an elbow type draft tube. Pressure and velocity measurements were carried out during steady-state operation (BEP and off-cam) [10-13]. Transient pressure measurements were also performed during load variations at a constant head value by Amiri et al. [14, 15]. The head of the turbine ($H$) is defined as:

$$H = \frac{(p_1 - p_2)}{\rho g} + \frac{Q^2}{2g} \cdot \left( \frac{1}{{A_1}^2} - \frac{1}{{A_2}^2} \right) + z_1 - z_2 \quad (1)$$

where $p_1$, $p_2$ represent the pressure at the inlet (1) and at the outlet (2) of the turbine respectively, $\rho$ is the fluid density, $g$ is the gravitational acceleration, $Q$ is the flow rate and $A_1$, $A_2$ are the surface areas of the guide vanes inlet (1) and draft tube outlet (2), $z_1$ and $z_2$ are the corresponding elevations.

The case chosen for the numerical simulations is the off-cam (fixed runner blades) load variation from BEP to part load operation (PL). The average angular velocity of the guide vane closing is $\omega_{GV}$ = 0.859 °/s. The load variation time is $\Delta t$ = 7.57 s. The parameters for the BEP and PL operating points, i.e. guide vane angle ($\alpha_{GV}$), flow rate ($Q$), and head ($H$) are presented in table 1.

**Table 1.** Operating parameters of the Porjus U9 model.

| Operating point | BEP | PL |
|---|---|---|
| $\alpha_{GV}$ (°) | 26.5 | 20 |
| $Q$ ($m^3/s$) | 0.69 | 0.62 |
| $H$ (m) | 7.5 | 7.5 |

### *2.2. Experimental data available for validation*

The transient numerical simulations are validated against velocity and pressure measurements performed in the runner by Amiri et al. [12, 13] and in the upper part of the draft tube cone by Mulu et al. [10, 11]. In the runner domain, 12 monitor points are defined according to the pressure sensors locations reported by Amiri et al. [13]. The uncertainties for the pressure sensors were ±0.3%. The locations of the monitor points on the runner blades are illustrated in figure 1.

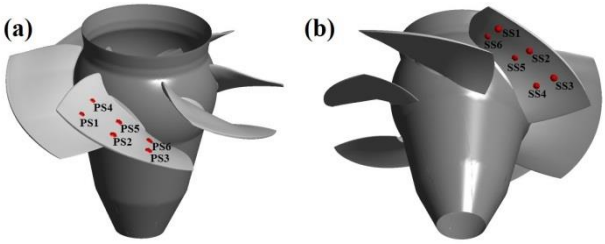


**Figure 1.** Pressure monitor points on the runner blades. **(a)** Pressure side (PS) on blade 1. **(b)** Suction side (SS) on blade 2.

Figure 2a presents the location of the monitor points corresponding to the pressure sensors as reported by Mulu et al. [10]. The monitor points are located on five levels (1 to 5) at four angular positions (a, b, c and d) as presented in figure 2b.

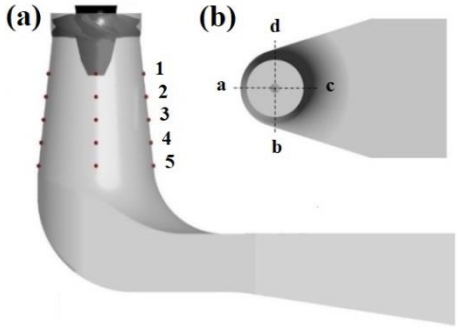


**Figure 2.** Pressure monitor points on the draft tube walls. (a) The positions of the pressure monitors are marked by red dots numbered from 1 to 5 starting from the top. (b) Circumferential positions.

Axial and tangential velocity profiles are obtained from Laser Doppler Anemometry (LDA) measurements performed by Amiri et al. [12] in the runner domain and by Mulu et al. [10, 11] inside the draft tube cone. The authors reported maximum uncertainties for the LDA measurements ranging from 0.65% to 1.4%. All velocity profiles are presented along the radius on direction d (figure 2b) based on the fact that the flow inside axial machines is axisymmetric. During the numerical simulation, the velocity is monitored using 20 monitor points defined along each red line (figure 3). The lines correspond to the LDA measurement sections located between the runner blades (section RB I), near the runner cone (section RC II) and in the draft tube cone (sections I to III).

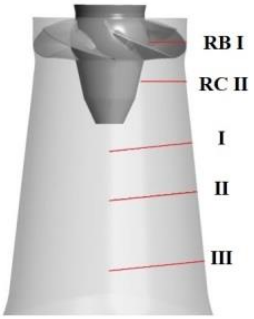


**Figure 3.** Velocity monitor points defined along the red lines: section RB I – between the runner blades, section RC II – below the runner blades, sections numbered I to III – in the draft tube cone.

*2.3. Numerical model*

Figure 4 presents the computational domain including one moving guide vane (GV), the complete runner (RN) composed of 6 runner blades and the elbow draft tube (DT). The configuration was chosen in order to capture the main flow parameters and characteristic inside the runner domain and

draft tube [20]. A Stage interface is defined between the guide vane domain and the runner domain. At the runner outlet, a Transient Rotor-Stator interface is employed in order to consider the transient relative motion between the runner and the draft tube. All simulations are performed using the Shear Stress Transport (SST) turbulence model. The SST model is a two-equation hybrid using the k-omega formulation in the inner region of the boundary layer and the k-epsilon model in the free shear flow. Two-equation RANS models are complete turbulence models, only requiring initial boundary conditions that provide a reasonable precision at low computational costs [21].

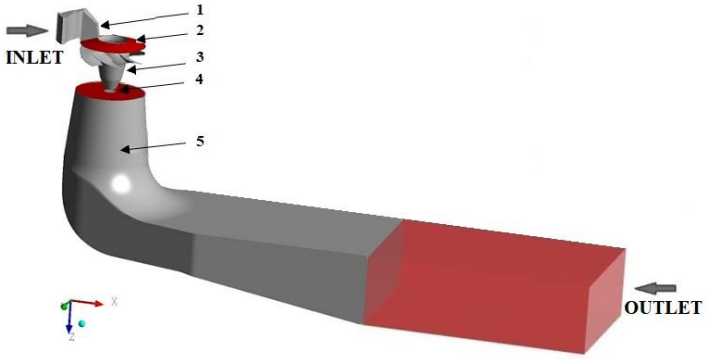


**Figure 4.** Computational domains and interfaces: 1. Guide vane domain. 2. Guide vane – runner interface. 3. Runner domain. 4. Runner – Draft tube interface. 5. Draft tube domain.

The mesh is created using ICEM 16.2. A hexahedral mesh is created for one runner blade passage, multiplied and rotated to ensure axial symmetry in the runner domain. The total number of cells in the entire Kaplan model domain is $6.48 \times 10^6$. The mesh properties, as they are evaluated by the CFX solver are presented in table 2. A mesh sensitivity analysis was previously performed by Mulu et al. [22] referring to the Porjus U9 draft tube mesh generated in ICEM. However, the runner mesh created in ICEM and used in the present numerical model is coarser than the mesh employed by Mulu et al. due to the complex geometry and the strict mesh quality criteria. The $y^+$ values are presented in table 2 along with the mesh quality parameters. The values are larger than the requirements of the SST turbulence model ($y^+<1$) and the automatic wall function is employed. In order to meet the $y^+<1$ criteria, a very fine mesh should be defined leading to a considerable increase in the mesh size along with the computational demands and the total simulation time.

**Table 2.** Quality parameters of the mesh used in the simulations.

| Domain | No. of elements [mil.] | Minimum angle [°] | Expansion factor | Aspect ratio | $y^+$ [-] |
|---|---|---|---|---|---|
| Guide vane | 0.18 | 20.2 | 16 | 58 | <165 |
| Runner | 2.64 | 16.8 | 48 | 668 | <235 |
| Draft tube | 3.66 | 30.5 | 9 | 7635 | <5 |

In order to model the guide vane rotation during closure, the mesh displacement is specified for the guide vane computational domain. The guide vane angle ($\delta\alpha_{GV}$) is calculated at each time step ($dt$) as:

$$\delta\alpha_{GV} = \omega_{GV} \cdot dt \cdot n \tag{2}$$

where $n$ is the current time step.

When setting the time step for a time dependent simulation, the smallest frequency of the system to be resolved must be considered. In order to choose an appropriate time step ($dt$), a sensitivity analysis is carried out. Unsteady simulations are performed for the different time step values presented in table 3. The larger time step values corresponding to the runner rotation angles $d\theta$ = 61 ° and $d\theta$ = 121° are chosen based on the hypothesis that the flow features around the blades are quasi-axisymmetric because all six runner blades are identical. The simulations are performed using the high resolution

scheme for the advection term and the second order backward Euler scheme for the time dependent terms in the RANS equations.

**Table 3.** Time step sensitivity analysis.

| Case | Time step $dt$ [s] | Corresponding runner rotation $d\theta$ [º] | Total simulation time [days] |
|---|---|---|---|
| 1 | 0.001195 | 5 | 20 |
| 2 | 0.014579 | 61 | 1.3 |
| 3 | 0.028919 | 121 | 0.9 |

The inlet boundary condition may be defined in terms of velocity (flow rate, mass flow rate or velocity profiles), static pressure or dynamic pressure. Mössinger et al. [19] found that the transient simulations using a linear flow variation as inlet boundary conditions during load variation were unable to predict the final pressure values. The authors suggested the total pressure should be specified at the inlet. For the present study, both types of inlet boundary conditions are investigated: a linear flow rate variation (referred to as: InletFlow simulation) and a constant total pressure throughout the entire load variation (referred to as: InletTotalPressure simulation). In the following sections, the variables with an index $Q$ and $P$ will refer to the InletFlow and InletTotalPressure simulation, respectively. The initial condition is a separate steady-state simulation of the turbine operating at BEP, performed with a constant inlet mass flow rate of 690 kg/s.

## 3. Results and discussion

The numerical values of the main parameters ($Q$ and $H$) obtained from the two transient simulations (InletFlow and InletTotalPressure) are compared for all time step values. The influence of the boundary conditions, i.e., a linear flow rate variation and a constant total pressure is discussed.

The averaged velocity profiles obtained from the steady-state simulations at the beginning (BEP) and the end of the transient simulation (PL) are compared to the experimental profiles in order to validate the numerical model. Results are presented for section RB I, in the runner blade channel and section I in the upper part of the draft tube cone (figure 3). All the velocity values are normalized using the bulk velocity calculated from the flow rate at BEP and the area at the corresponding section. The radii are made dimensionless relative to the runner radius $R$ = 0.25 m.

The pressure results provided by monitor points on the runner blade (PS1) and the draft tube wall (3c) are presented. The influence of the time step size over the amplitude of the pressure fluctuations is investigated.

### *3.1. Boundary condition influence*

The time variations of the guide vane angle ($\alpha_{GV}$), flow rate ($Q$) and head ($H$) obtained from the transient numerical simulations (InletFlow and InletTotalPressure) are presented in figure 5. The values represent percentages out of the BEP steady-state experimental operating parameters. At the beginning of the simulations, i.e., the steady-state initial condition, the turbine is operating at the BEP. After $t_1$ = 1.3 s, the closure of the guide vane begins. The guide vane rotates 6.5 ° during $\Delta t$ = 7.57 s. The flow rate decreases gradually and the PL operation is reached at $t_2$ = 8.87 s.

At PL, the flow rate predicted by the InletFlow simulations represents 90% of the BEP value matching as expected, the experimental value that was provided as inlet boundary condition. When using the total constant pressure as an inlet boundary condition, the flow rate is underestimated. During the guide vane closure, the difference between the flow rate values provided by the two simulations is observed after $t$ = 3.3 s (red vertical line in figure 5a) and increases from 0 to 6.5%. At PL, the InletTotalPressure simulation predicts an average flow rate of 84.5% of the BEP value (figure 5a). RANS turbulence models are dissipative in the sense that they overpredict the pressure losses due to the limited modelling of the near-wall flows with large pressure gradients, complex geometry and

strong curvature [23]. Therefore, for a fixed head value provided as an inlet boundary condition, the SST turbulence model underestimates the flow rate.

A similar behaviour is observed when analysing the variation of the numerically obtained head values during the same transient operation (figure 5b). Due to the numerical overestimation of the pressure losses, when providing the flow rate as an initial boundary condition, the numerical model will overpredict the total head required to maintain the flow rate. The values of the turbine head defined as boundary conditions are larger than the reported measurements (125%) because they were chosen from the steady-state simulations instead of using the experimental values. This was decided in an attempt to capture the correct flow rate variation considering the known overestimation of the pressure losses that characterizes URANS simulations. Despite defining a numerically obtained total pressure as the inlet boundary condition, the flow rate is underestimated starting from approximately 2 seconds after the beginning of the load variation (red vertical line in figure 5b). The deviation from the InletFlow simulation becomes larger during the load variation and stabilizes after reaching the PL steady-state operation.

The time step size has a very small influence over the flow rate and head values obtained from the numerical simulations. Therefore, the main flow features can be accurately captured at large time step values based on the hypothesis that the flow is quasi-axisymmetric, saving simulation time and computational resources.

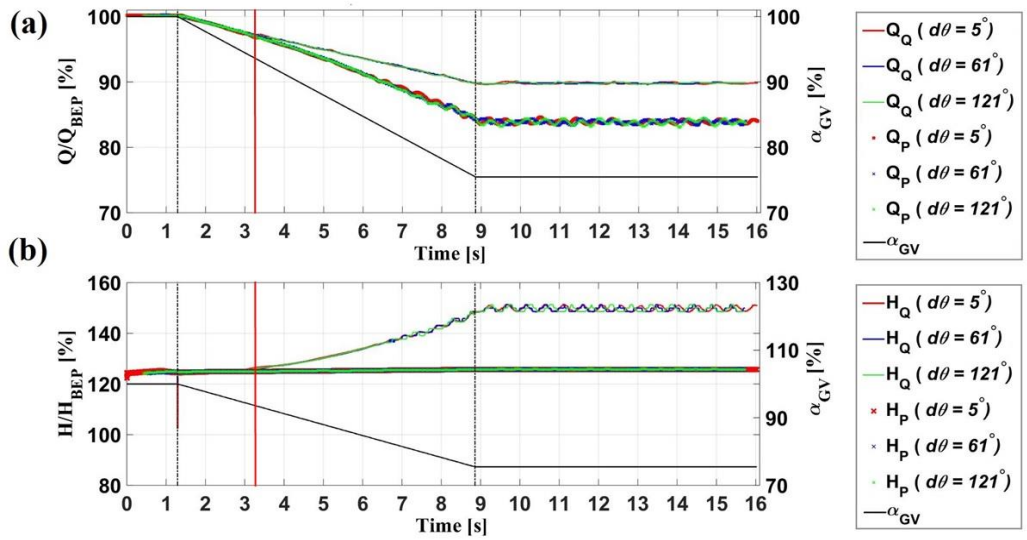


**Figure 5. (a)** Time-dependent variation in the guide vane angle and discharge ($Q$) during the load variation. **(b)** Time-dependent variation of the head ($H$). The black dotted vertical lines represent the start ($t_1$) and the end ($t_2$) of the guide vane closure.

*3.2. Velocity profiles*

Figure 6 presents the results obtained from numerical simulations during the BEP steady-state operation. The velocity profiles are averaged over 15 runner rotations. These unsteady simulations were performed in order to provide the initial conditions for the transient simulation. The mass flow rate was defined as the inlet boundary condition.

In the runner domain, section RB I (figure 3) the numerical simulations provide results very similar to the experiments. At BEP, the flow is following the geometry. In the centre of the draft tube cone, just below the runner hub (section I in figure 3), the flow is not captured correctly regardless of the time step size. The tangential velocity is overestimated near the axis of the draft tube, leading to an underestimation of the axial velocity down to negative values due to the conservation of the flow rate. The simulations show that a recirculation area forms at the inlet of the draft tube even during BEP operation. Towards the draft tube wall, both the axial and tangential velocity profiles match the measurements.

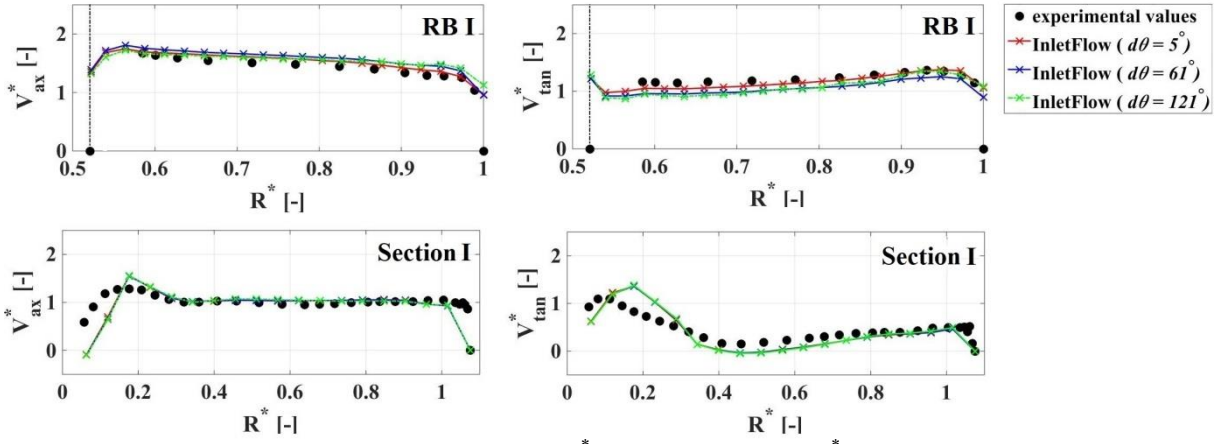


**Figure 6.** Experimental and simulated axial ($V_{ax}^*$) and tangential ($V_{tan}^*$) velocity at BEP, in the runner blade channel (section RB I) and below the runner hub (section I). The dotted vertical lines represent the hub wall.

Figure 7 presents the results obtained from the numerical simulations during the PL steady-state operation. The velocity profiles are averaged over 80÷83 runner rotations (depending on the time step value). At PL, the angle of the flow reaching the runner blades is not optimal. The flow becomes more complex as secondary flows develop and the frequency of the turbulent fluctuations increases. Therefore, finding a good agreement between the numerical simulations and the experimental values is more difficult.

In the runner blade channel, the velocity profiles obtained from the simulations are similar for both types of boundary conditions. The axial velocity is slightly overestimated as opposed to the tangential velocity which is underestimated by up to 15%. Neither of the two simulations can capture the high axial velocity near the shroud wall (clearance jet) during PL operation despite the blade clearances being modelled. Further downstream in the draft tube cone, the differences become visible. Near the centre of the draft tube, all simulations underestimate the axial velocity. The InletFlow simulations provide the results closest to the measurements. In this area, the time step size influence is visible but no conclusion can be drawn from these profiles. The simulation using the smallest time step corresponding to 5° of the runner rotation captures best the axial velocity but not the tangential velocity. Towards the draft tube wall, the InletFlow simulations agree regardless of the time step size and match the measurements.

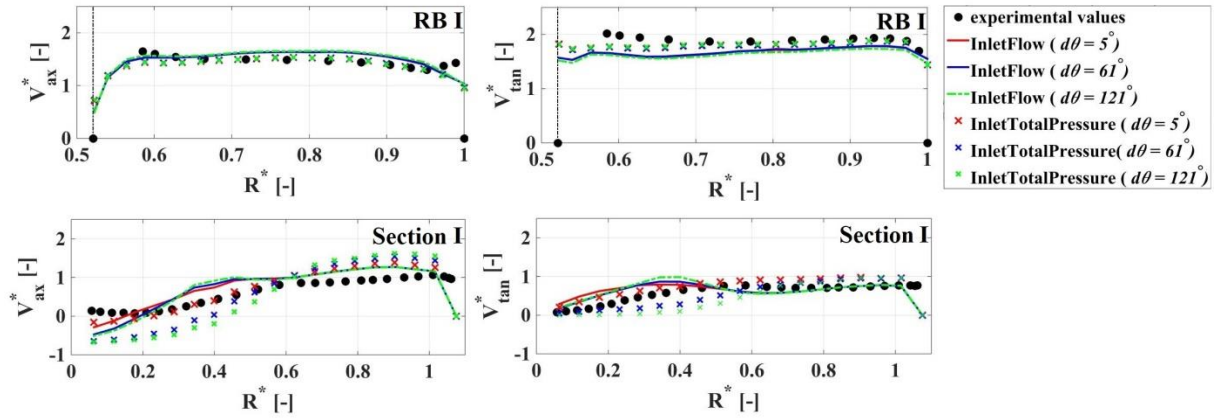


**Figure 7.** Experimental and simulated axial ($V_{ax}^*$) and tangential ($V_{tan}^*$) velocity at PL, in the runner blade channel (section RB I) and below the runner hub (section I). The dotted vertical lines represent the hub wall.

*3.3. Pressure oscillations*

Depending on the type of boundary conditions defined for the inlet of the computational domain, the numerical simulations show different evolutions of the pressure fluctuations in time, as presented in figure 8. Inside the runner domain (figure 8a) the InletFlow simulation overpredicts the pressure values to maintain the fixed flow rate value defined at the inlet of the guide vane. The larger pressure values compensate for the pressure losses overestimated by the numerical model. Downstream, in the draft tube domain, this difference between the absolute pressure values is no longer visible. However, the amplitudes of the pressure fluctuations obtained during the guide vane closure by the monitor points defined on the draft tube wall are different for the two types of simulations. As mentioned before, the InletTotalPressure simulation is overestimating the losses and therefore, underestimating the flow rate. This conclusion is consistent with the observations from figure 5, where the underestimation of the flow rate becomes visible approximately 2 seconds after the start of the guide vane closure. As a consequence, the pressure fluctuations with large amplitudes are noticed earlier in the InletTotalPressure simulation (figure 8b). The time step size also has a strong influence on the amplitudes of the pressure fluctuations, especially in the InletTotalPressure simulation.

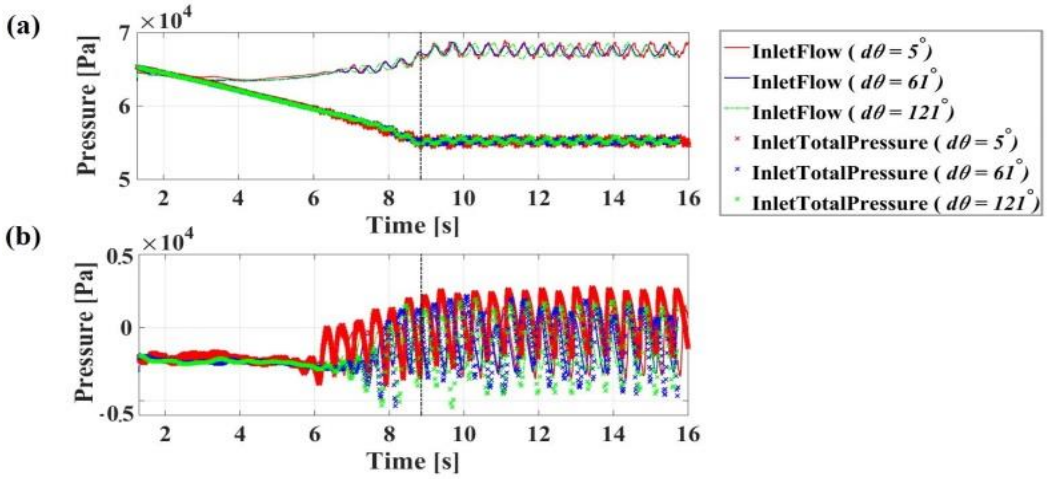


**Figure 8.** Pressure-time variation; comparison between the numerical simulations: (a) monitor point PS1 in the runner domain and (b) monitor point 3c in the draft tube domain. The dotted vertical line represents the end ($t_2$) of the transient operation.

As expected, the simulated pressure fluctuations are larger when the time step decreases. The cause of such behaviour could be that the high frequency associated to the small time step, $f_1$ = 836 Hz, falls in the turbulent frequency spectrum. In this case, the turbulent fluctuations are resolved from the lowest turbulent frequency $f_{min} = v/D \approx 8$ Hz up to half of the sampling frequency $f_1/2$= 418 Hz. On the other hand, when using larger time steps with the corresponding sampling frequencies of $f_2$ = 68 Hz and $f_3$ = 34 Hz respectively, a larger part of the turbulent fluctuations are modelled and therefore damped due to an overestimation of the pressure losses.

Figure 9 presents a Fast Fourier Transform (FFT) analysis of the simulated pressure on the runner blade for all time step sizes. Only the results of the InletFlow simulation are presented. The frequency is normalized using the runner rotational frequency $f_{runner}$ = 11.61 Hz. The pressure peaks are captured at the same dimensionless frequency values but show very different amplitudes depending of the time step size. Two amplitude peaks are showed in figure 10a indicating the presence of the rotating vortex rope (RVR) that is developing inside the draft tube during the guide vane closure. All simulations show the first peak at 0.18 $f_{runner}$ corresponding to the synchronous mode of the RVR and the second at 0.82 $f_{runner}$ corresponding to the RVR asynchronous mode [4, 11]. In figure 9b the monitor point located on the draft tube wall (stationary frame of reference) shows the simulations still captures the RVR rotational frequency of 0.18 $f_{runner}$. The amplitudes of the pressure fluctuations are however strongly influenced by the time step size.

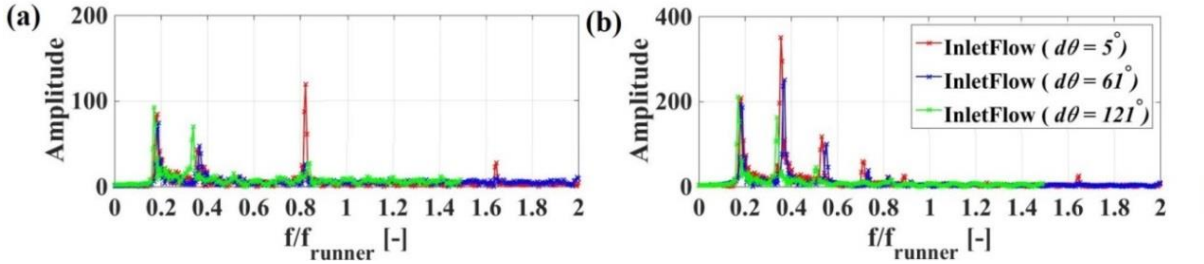


**Figure 9.** Amplitude spectra of the numerical pressure signal recorded throughout the load variation and PL operation. (a) Monitor point PS1 near the leading edge, on the pressure side of the blade. (b) Monitor point 3c on the draft tube cone wall.

## 4. Conclusions

Transient URANS simulations of the flow through an axial hydraulic turbine were performed. The aim of the paper was to evaluate the limitations of CFD numerical modelling concerning transient simulations with a specified mesh displacement. The test case was the Porjus U9 Kaplan turbine model operated off-cam during load variation from BEP to PL. The computational domain included one moving guide vane, six runner blades and the draft tube.

The influence of the inlet boundary conditions on the accuracy of transient simulations was discussed. Two types of boundary conditions were defined at the inlet of the guide vane: a linear flow rate variation and a constant total pressure. The InletFlow simulation overpredicted the pressure values in the runner domain due to the numerical overestimation of the pressure losses. When, on the other hand, the constant total pressure was fixed, the flow rate was underestimated by up to 6%.

Concerning the velocity profiles presented in the runner and draft tube, a reasonable match with the experimental results was obtained for both types of inlet boundary conditions employed for the BEP simulations. At PL however, the InletFlow simulations provided a better agreement to the measurements compared to the InletTotalPressure simulations.

A time step sensitivity analysis was also performed in the attempt to obtain a shorter simulation time while maintaining a good accuracy of the results. The main parameters of the flow were not influenced by the time step size. The pressure fluctuations recorded on the runner blade were analysed; as expected, the small time step size provided large amplitude fluctuations of the pressure values. The high frequency corresponding to a small time step may fall in the turbulence frequency spectrum and therefore lead to the resolving of the turbulent fluctuations and the overestimation of their amplitudes. A simulation using a very large time step will, on the other hand, only provide mean values of the pressure oscillations.

Results showed that considering the available CFD procedures it is still challenging to create realistic numerical models of transient turbulent flows. RANS numerical models overpredict the head losses regardless of the type of boundary condition.

## References

[1] Trivedi C, Cervantes M J and Dahlhaug O G 2016 Experimental and numerical studies of a high-head Francis turbine: a review of the Francis-99 test case, *Energies*, **9(2)**, 74.

[2] Houde S, Fraser R, Ciocan G D and Deschênes C 2012 Part 1 - Experimental study of the pressure fluctuations on propeller turbine runner blades during steady-state operation, *Earth Environ. Sci.*, **15**.

[3] Houde S, Fraser R, Ciocan G D, Deschênes C 2012 Experimental study of the pressure fluctuations on propeller turbine runner blades: Part 2, transient conditions, *Earth Environ. Sci.*, **15**.

[4] Goyal R, Bergan C, Cervantes M J, Gandhi K and Dahlhaug O G 2016 Experimental investigation on a high head model Francis turbine during load rejection, *Earth Environ. Sci.,* **49**.

[5] Trivedi C, Cervantes M J, Gandhi B K and Dahlhaug O G 2014 Transient pressure

measurements on a high head model Francis turbine during emergency shutdown, total load rejection, and runaway, *J. of Fl. Eng.*, **136(12)**.

[6] Coulaud M, Fraser R, Lemay J, Duquesne P, Aeschlimann V, Deschênes C 2016 Preliminary investigation of flow dynamics during the startup of a bulb turbine model, *Earth Environ. Sci.*, **49**.

[7] Mulu B, Jonsson P and Cervantes M J 2012 Experimental investigation of a Kaplan draft tube - Part I: Best efficiency point, *Applied Energy*, **93**, 695-706.

[8] Jonsson P, Mulu B and Cervantes M J 2012 Experimental investigation of a Kaplan draft tube Part II: Off-design conditions, *Applied Energy*, **94**, 71–83.

[9] Amiri K, Mulu B and Cervantes M J 2016 Experimental investigation of the interblade flow in a Kaplan runner at several operating points using Laser Doppler Anemometry, *J. of Fluids Eng.,* **138(2)**.

[10] Amiri K, Cervantes M J and Mulu B 2015 Experimental investigation of the hydraulic loads on the runner of a Kaplan turbine model and the corresponding prototype, *J. of Hydraulic Research*, **53(4)**, 452-465.

[11] Amiri K, Mulu B, Raisee M and Cervantes M J 2016 Unsteady pressure measurements on the runner of a Kaplan turbine during load acceptance and load rejection, *J. of Hydraulic Research*, **54(1)**, 56-73.

[12] Amiri K, Mulu B, Cervantes M J and Raisee M 2016 Effects of load variation on a Kaplan turbine runner, *J. of Fluid Machinery and Systems*, **9(2)**, 182-193.

[13] Keck H and Sick M 2008 Thirty years of numerical flow simulation in hydraulic turbomachines, *Acta Mechanica*, **201(1)**, 211–229.

[14] Pinto R N, Afzal A, D'Souza L V, Ansari Z and Samee A D M 2016 Computational Fluid Dynamics in turbomachinery: a review of state of the art, *Archives of Computational Methods in Engineering,* 1-13.

[15] Ko P and Kurosawa S 2014 Numerical simulation of turbulence flow in a Kaplan turbine - Evaluation on turbine performance prediction accuracy, *IOP Conf. Series: Earth Environ. Sci.*, **22**.

[16] Goyal R, Trivedi C, Gandhi B K, Cervantes M J 2017 Numerical simulation and validation of a high head model Francis turbine at part load operating condition, *J. of The Institution of Engineers (India): Series C*, 1-14.

[17] Mössinger P, Jester-Zürker R, Jung A 2017 Francis-99: Transient CFD simulation of load changes and turbine shutdown in a model sized high-head Francis turbine, *J. of Phys. Conf. Series*, **782**.

[18] Nicolle J, Giroux A M, Morissette J F 2014 CFD configurations for hydraulic turbine startup. *Earth Environ. Sci.*, **22**.

[19] Wilhelm S, Balarac G, Metais O, Segoufin C 2016 Analysis of head losses in a turbine draft tube by means of 3D unsteady simulations, *Flow, Turbulence and Combustion*.

[20] Gagnon J M, Flemming F, Qian R Deschênes C, Coulson S 2010 Experimental and numerical investigations of inlet boundary conditions for a propeller turbine draft tube, *ASME 3rd Joint US-European Fl. Eng. Summer Meeting*, **1**.

[21] Alfonsi G 2009 Reynolds-averaged Navier-Stokes equations for turbulence modeling, *Applied Mechanical Reviews*, **62(4)**.

[22] Mulu B, Cervantes M J, Vu T, Devals C and Guibault F 2015 Simulation-based investigation of unsteady flow in near-hub region of a Kaplan turbine with experimental comparison, *Eng. Appl. of Computational Fl. Mech.*, **9(1)**, 139-156.

[23] Smirnov P and Menter F 2009 Sensitization of the SST turbulence model to rotation and curvature by applying the Spalart-Shur correction term, *J. of Turbomachinery*, **131**.